Estimation of the Frequency-Dependent Shear Wave Attenuation from Acceleration Spectra of the Ahar-Varzeghan Earthquake 2012

Saman Amiri[1], Majid Mahood[2], and Hossein Hamzehloo[3]*

1. M.Sc. Graduate in Earthquake Engineering, International Institute of Earthquake Engineering and Seismology (IIEES), Tehran, Iran
2. Assistant Professor, Seismology Research Center, International Institute of Earthquake Engineering and Seismology (IIEES), Tehran, Iran,
* Corresponding Author; email: m.mahood@iiees.ac.ir
3. Professor, Seismology Research Center, International Institute of Earthquake Engineering and Seismology (IIEES), Tehran, Iran

ABSTRACT

Two destructive earthquakes occurred on 11th of August 2012 (Mw 6.5 and 6.4) in the Ahar and Varzeghan regions, NW Iran. High-frequency strong-motion data of these earthquakes have been analyzed to determine the $Q_\beta(f)$ and source parameters by inversion of the recorded data. The data from a local network of 21 and 19 acceleration records for the first and second main shocks have been used to estimate Q-relationship in 30 stations. The seismic hazard map for this region illustrates that most of the area in this province is located within high relative risk and characterized by a large number of heterogeneities. For frequency band of 1 to 20 HZ, the frequency-dependent attenuation for this region has been estimated. The authenticity of achieved $Q_\beta(f)$ relation is checked by comparing the source spectra in various stations with the theoretical spectra. Low values of the coefficient (Q<200) in the $Q_\beta(f)$ relation suggest that the region is seismically and tectonically active. The present inversion of strong-motion data gives the source parameters i.e. corner frequencies and stress drops as f_{c1}= 0.08 Hz, f_{c2}= 0.11 Hz, $\Delta\sigma_1$=77.14 bar and $\Delta\sigma_2$=33.06 bar, respectively.

1. Introduction

In this study, the focus is on the attenuation characteristics of the North-West of Iran. The knowledge of attenuation properties within the media is required for investigation of earth structure and seismotectonic activity. Besides, $Q_\beta(f)$ is an important physical parameter and is required for successful simulation of strong ground motion using different techniques such as semi empirical modeling, composite source modeling and stochastic simulation. Attenuation of seismic waves with frequency depends strongly on the physical conditions of the underground crustal media. Tectonic activities can change the stress fields, which will result in the geo-morphological deformation within the media and cause micro-fractures, brittle zone and fault zones. These fractures can change the attenuation properties of a media. The change in the attenuation characteristics with time may be

attributed to an increase of pressure in the crust producing new cracks and/or reopening of pre-existing cracks, which are the most viable mechanisms for increasing attenuation [1]. Therefore, a good physical agreement can be expected between attenuation properties, seismicity and tectonics [2].

Recently, a technique has been developed by Joshi [3] that uses the S-phase of an accelerogram as an input in an inversion algorithm and gives $Q_\beta(f)$ and corner frequency, f_c, of the input events. The approach suggested by Joshi and subsequently modified by Joshi et al. [4] was applied to calculate the $Q_\beta(f)$ and source parameters. Kumar et al. [5] studied shear wave attenuation by using the modified inversion of strong-motion data in the Kumaon Himalaya, India. For the S-waves at frequencies 1 to 25 Hz, Q_β is proportional to f^n where the range of n differs between 0.6 and 0.8 on average [2, 6]. The frequency-dependent Q-relationship can be used to characterize the tectonic nature of the region. The relation $Q = Q_0 f^n$ in general provides Q_0, which represents heterogeneities, and n represents the level of tectonic activity of the region. The regions with higher n value manifest the higher tectonic activity. Worldwide result show low values of Q_0 (<200) for tectonically and seismically active regions, high Q_0 (>600) for the stable regions and intermediate values for the moderate regions [7-8].

Table (1) presents a comparative list of worldwide $Q_\beta(f)$ relationships. As it can be seen, low value of Q in north-west of Turkey illustrates tectonically and seismically active while the central United States [9] and NE-US [10] with high Q_0 are representative for stable regions.

Many researchers have used different techniques to determine seismic parameters in Iran. Zafarani was one of the pioneers in estimating source parameters by using inversion method in Iran. Earthquake parameters and shear wave attenuation have been calculated by Zafarani et al. [13] in Alborz seismic zone. For the East-Central Iran, Mahood and Hamzehloo [8, 12] estimated the coda wave attenuation and high frequency S-waves attenuation, respectively, which depict on Table (1). Hassani et al. [14] estimated site amplification, attenuation and source spectra of S-waves in the East-Central Iran. Motaghi and Ghods [15] studied the attenuation of ground-motion spectral amplitudes

Table 1. Comparative list of $Q(f)$ relationships in worldwide range.

Active Region	$Q(f)$ Relationship	Reference
Alborz	$Q(f) = 111 f^{0.85}$	Farokhi et al. [11]
NE-US	$Q(f) = 1052 f^{0.22}$	Benz et al. [10]
Eastern Iran	$Q(f) = 75 f^{1.03}$	Mahood [1]
East-Central Iran	$Q(f) = 131 f^{1.01}$	Mahood and Hamzehloo [12]
South-East of Iran	$Q(f) = 99 f^{0.5}$	Safarshahi et al. [41]
South Korea	$Q(f) = 333 f^{0.42}$	Kim et al. [40]
Alborz	$Q(f) = 101 f^{0.8}$	Zafarani et al. [13]
East-Central Iran	$Q(f) = 151 f^{0.75}$	Hassani et al. [14]
Himalaya	$Q(f) = 112 f^{0.97}$	Anand Joshi (2007) [42]
North-West of Turkey	$Q(f) = 17 f^{0.8}$	Bindi et al. (2006) [43]
The Central United States	$Q(f) = 640 f^{0.34}$	Erickson et al. (2004) [9]

and its variations across the central Alborz Mountains. Rahimi et al. [16] and Farrokhi et al. [17] estimated coda-wave attenuation in the central and eastern Alborz. Farrokhi and Hamzehloo [11] investigated body wave attenuation characteristics in the Alborz region and north central Iran. In the NW-Iran, however, a few works has been performed. Zafarani et al. [18] found the frequency-dependent S-wave quality factor, $Q_s = 99 f^{0.77}$ from the stochastic simulation of strong-motion records of the Ahar-Varzeghan earthquakes. The generalized inversion of S-wave amplitude spectra is employed for deriving the site response and S-wave attenuation (Q_s) in the NW-Iran by utilizing two main shocks of Ahar and Varzeghan and 40 accelerograms. The significant difference between this study and previous one is that unlike Zafarani et al. [18], in this study, Andrews [19] formula is used in order to calculate corner frequency and subsequently, other source parameters. Furthermore, singular inversion has been used for determining all stations separately in order to find Q value for each station. In addition, the effects of Sahand and Sabalan volcanoes on Q-value analyzed based on Dell Pezzo et al. [20] in south of Spain, which illustrate values of Q for near volcanoes stations are slightly smaller than those measured in non-volcanic zones.

The main objective of this article is to obtain $Q_\beta(f)$ relation for NW-Iran from the inversion of acceleration spectra at all stations and to compute the source parameters of earthquakes. The source spectrum has important information of earthquake

source and wave propagation medium; therefore, it is directly employed to compute various source parameters like stress drop, seismic moment and source radius. The advantage of using the strong-motion data for the inversion is high-frequency content of near-field data that is valuable for engineering purposes.

2. Tectonic Setting and Seismic Activity

Iran lies within the complex zone of continental collision between the Arabian and the Eurasian Plates, which extends from the Bitlis-Zagros belt in the south to the Greater Caucasus mountains, the Absheron-Balkan Sill and the Kopehdagh mountains in the north. The collision between these plates is one of the largest convergent deformation regions on the Earth. In NW-Iran, the Arabian Plate is moving northwards about 20 mm/yr relative to the Eurasian Plate, somewhat oblique to the plate boundary zone [21]. The deformation in the area near Tabriz is dominated by the North Tabriz Fault, a WNW-ESE trending right-lateral strike-slip fault, which has been responsible for seven historical earthquakes with magnitude of $M > 6$ since AD 858. Other known active faults include a W-E trending fault between the cities of Ahar and Heris.

The wider tectonics of the Arabia-Eurasia collision zone at the NW-Iran and east of Turkey is characterized by right-lateral strike-slip faulting on WNW-ESE planes in the Turkish-Iranian Plateau, and thrust faulting with the same strike in the Greater Caucasus further north (Figure 1a). This arrangement of faulting accommodates the oblique northwestward convergence of Arabia with Eurasia by the spatial separation (partitioning) of the faults accommodating the strike-slip and shortening components of motion [22-24]. The partitioning of thrust and strike-slip faulting in this way can also clearly be seen in the Global Positioning System (GPS) velocities shown in (Figure 1b) [25-27]. Strike-slip faulting within the Turkish-Iranian Plateau accommodates the change in motion relative to Eurasia from NNW in the south near Lake Urmia (LU in Figure 1b) to NE in the northern part of the plateau. The Ahar-Varzeghan earthquakes are within the zone of right-lateral strike-slip faulting in the Turkish-Iranian Plateau that accommodates the strike-slip component of the overall Arabia-Eurasia relative motion (Figure 1).
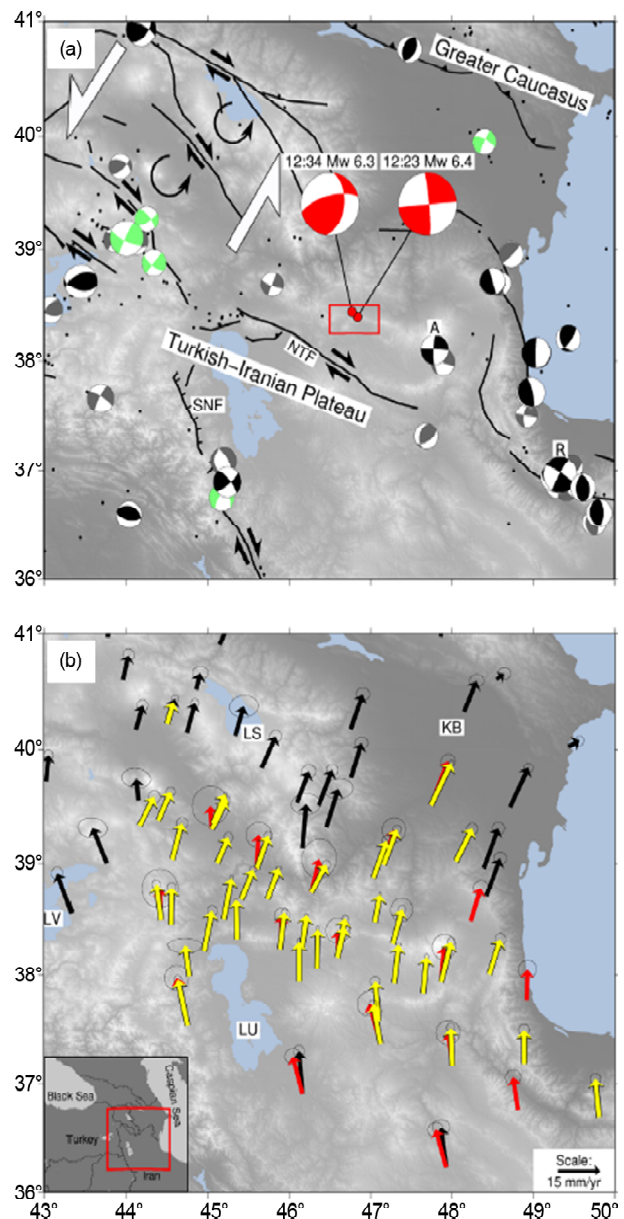

Figure 1. (a) Earthquakes in the Turkish-Iranian Plateau [inset to (b) shows the area of coverage and national borders]. Black dots are earthquakes in the EHB catalogue, green focal mechanisms are from first motions, grey are global CMT solutions (www.globalcmt.org) and black are from modeling of P and SH waveforms [from Elliott et al. [44] and the compilation of Copley and Jackson [24]. The two red focal mechanisms represent the 2012 Ahar events. The 12:23 mechanism is from our waveform modeling, and the 12:34 mechanism is the global CMT solution. 'A' shows the 1997 Mw 6.0 Ardebil earthquake, 'R' shows the 1990 Mw 7.3 Rudbar earthquake, NTF shows the North Tabriz Fault and SNF represents the Serow normal faults. Mapped faults are from Jackson et al. [45] and Copley and Jackson [24]. Large white arrows show the overall right-lateral shear on NE/SW planes in the northern Turkish-Iranian Plateau, which is accommodated by anticlockwise rotations (black-curved arrows) and right-lateral strike-slip faulting [24]. The red box shows the area of coverage of Figure 1. (b) GPS velocities relative to Eurasia from Reilinger et al. [26] (black), Masson et al. [25] (red) and Djamour et al. [27] (yellow). LU, LV and LS represent lakes Urumiyeh, Van and Sevan. KB shows the Kura Basin.

3. Data Set

Ahar-Varzeghan earthquakes shook the NW Iran at 12:23 UTC on August 11, 2012 (Figure 1). It was followed 11 min later by a second event of comparable size, 6.4 Mw (Figure 2). The casualties were announced as 872 dead and more than 3000 injuries during these two destructive earthquakes, and several houses were damaged [28].The comparable magnitudes of these events and their close spatial and temporal relationship justify treating them as an earthquake doublet [29]. The doublet main shocks have 48 and 62 accelerograms of BHRC (Building and Housing Research Center), respectively. All instruments were composed of SSA-2 digital accelerographs with a 10-Gal (0.1 m/s^2) threshold, sampling rate of 200 samples/s, and natural frequency of 50 Hz.

We have considered 40 recorded time histories with a good signal-to-noise ratio (*S/N*>3) and with epicentral distance, *R*<120 km. Therefore, in this study, 21 and 19 high-frequency acceleration spectra are used for the two earthquakes, respectively. Figure (2) illustrates earthquake epicenters and the locations of the accelerograms stations.

4. Methodology

4.1. Temporarily Qp Estimation

Coda waves provide a reliable way to isolate and quantify seismic propagation effects. Based on the single scattering model, the average coda amplitude at a long lapse time t_c from the origin time at central frequency *f* is as a product of the source, propagation and site amplification. Aki [6] proposed a correction for source size and site amplification by normalizing direct S-wave amplitude by S-coda amplitude. He first used this method for the estimation of Q_s in Japan. This method was extended by Yoshimoto et al. [30] to measure Q_p for Kanto, Japan. They assumed that for a small magnitude range, 2.5 to 4.5, the ratio of P- to S-wave source spectra is constant. One reason that the coda normalization method has been so useful is because the station calibration and/or site amplification could be eliminated so that other medium parameters could be measured. According to Yoshimoto et al. [30], we can measure the quality factor of the direct P-waves from the seismogram of earthquakes observed at different hypocentral distances by using Equation (1):
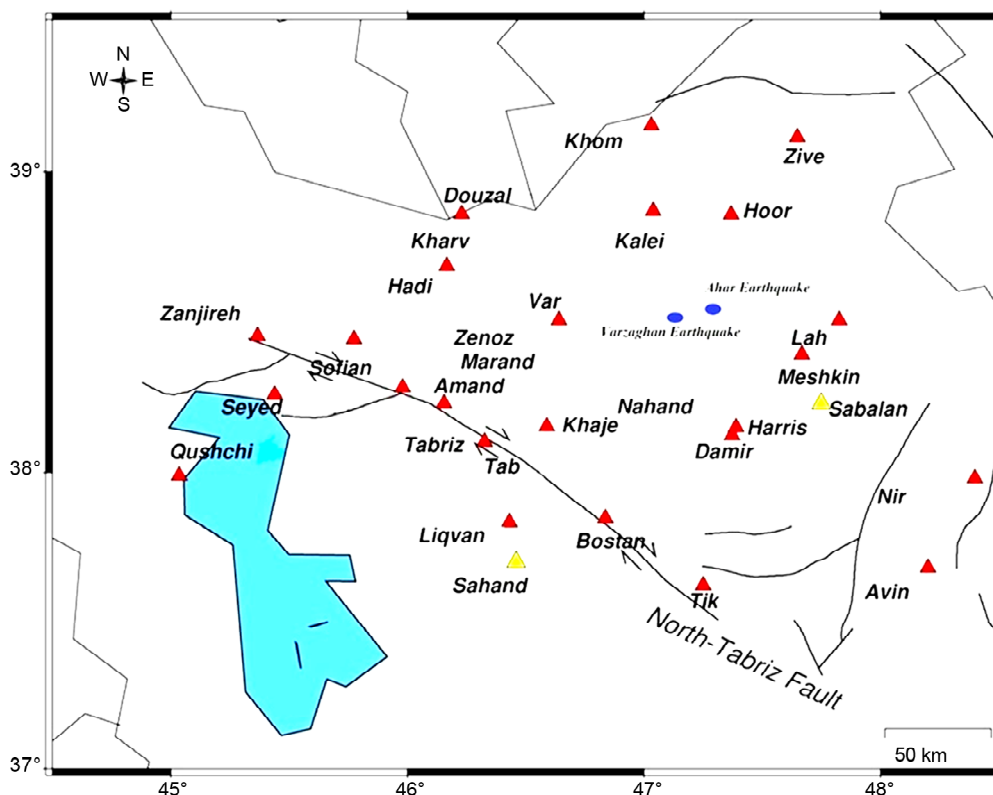

Figure 2. An overview of NW-Iran with the Ahar-Varzeghan earthquakes (blue elliptic), strong motion some stations (red triangles), Sahand and Sabalan volcanoes (yellow triangles) and active faults.

$$\ln\left[\frac{A_p(f,r)r}{c(f,t_c)}\right] = -\frac{\pi f}{Q_p(f)V_p}r + const(f) \qquad (1)$$

where f is frequency and t_c is a fixed lapse time from the origin time, r is the hypocentral distance, $V_p = 6.5$ km/s; $A_p(f,r)$ is the P-wave maximum amplitude, which is measured in a 5-s time window starting from the onset of P -waves on the filtered seismograms.

$c(f,t_c)$ is the coda spectral amplitude, which was assumed to be the rms of the amplitude of the seismic wave within the 5-s time window after the 50-s lapse time ($t_c = 50$ s). Generally, tc at later time was difficult to obtain due to the noise problem or recording time [1]. Figure (3) shows a mean value of Q_p and the standard deviations represented by error bars.
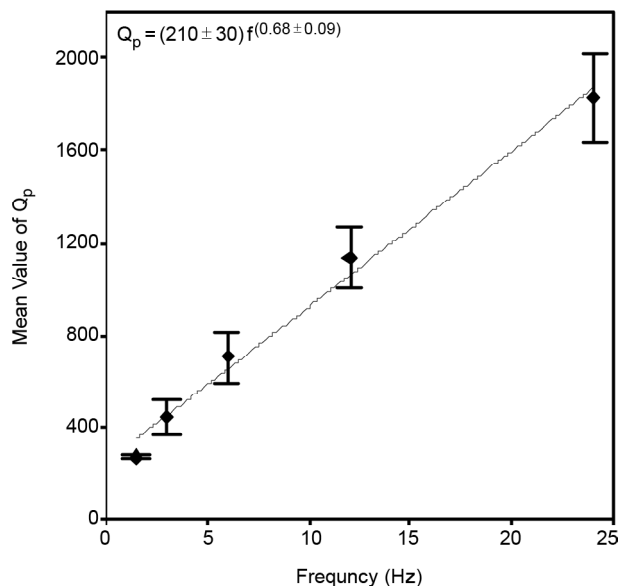

Figure 3. Mean value of Q_p with best-fit power-law lines. The standard deviations represented by error bars.

4.2. Source Parameters

Inversion analysis is based on detection of S-wave window and the S-wave analysis was based on the SH-waves synthesized from horizontal components, because SH-waves are not affected by other seismic phases. For separating S-wave window, Kinoshita [31] method is used for determining the end of S-wave time window analysis, in this research. Besides, take start of energy descent in diagram by using Butterworth 4-pole filter and in frequency band between 0.01 to 20 HZ (Figure 4). For an accelerogram, $a(n)$ is amplitude of corrected
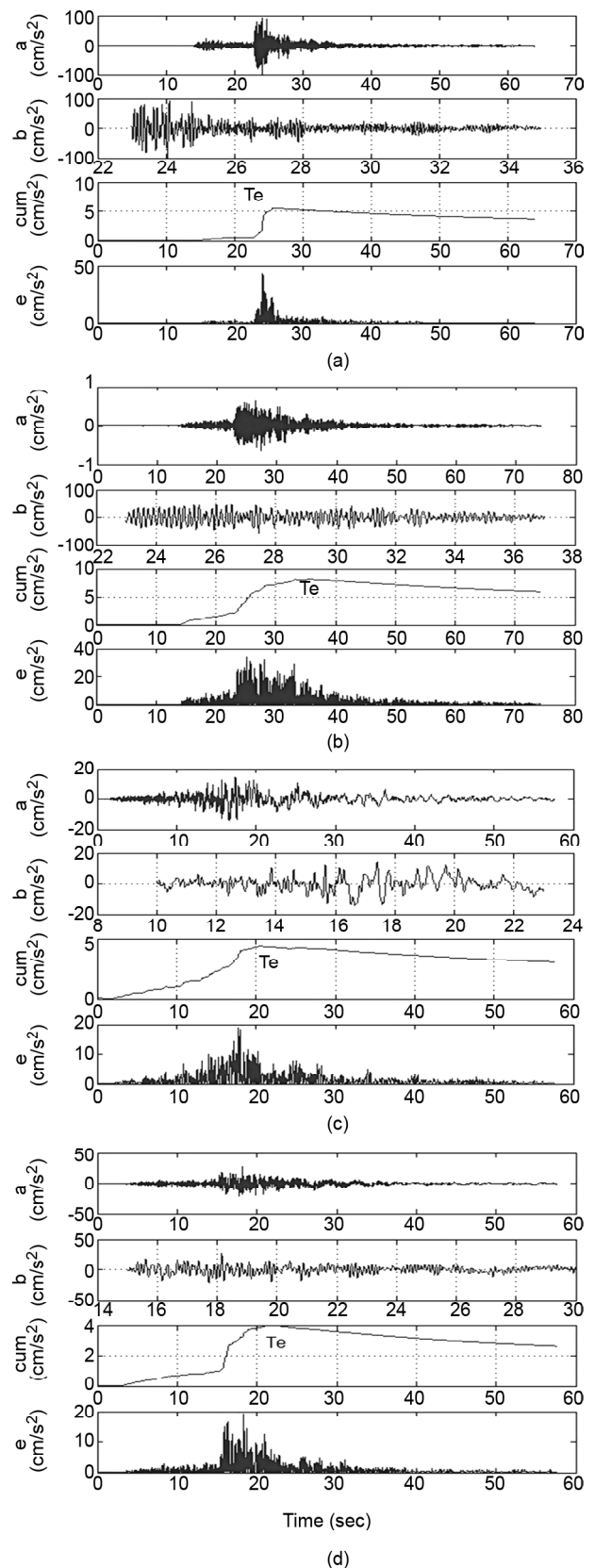

Figure 4. Selected portions of longitudinal components of accelerograms of the Ahar-Varzeghan Earthquakes detected S-Waves by using Kinoshita [31]. In the Kinoshita method, the ending time, Te, of the S-wave window is assigned to a point on the time axis where c(k) starts to decrease. Plot shows acceleration records at (a) Douzal, (b) Hoorand, (c) Bostan Abad, (d) Khoomarloo stations.

record, $b(n)$ is S-wave time window and acceleration envelope, $e(n)$, is obtained by the following equation:

$$e(n) = [b(n)^2 + H^2(b(n))]^{0.5} \qquad (2)$$

where $H\{b(n)\}$ denotes the Hilbert transform of $b(n)$. Then, the cumulative rms function $c(k)$ is calculated from $e(n)$ as:

$$c(k) = [k^{-1} \sum_{n=1}^{k} e(n)^2]^{0.5} \qquad (3)$$

In the Kinoshita method, the ending time, $T(e)$, of the S-wave window is assigned to a point on the time axis where $c(k)$ starts to decrease.

Using Andrews [19] formula the corner frequency of the SH-waves for each station has been calculated (Table 2). Due to the average of the corner frequency, M_0, the radius of circular rupture (r_0) and stress drop for events are calculated. The corner frequency was computed with the formula introduced by Andrews [19]:

$$f_c = \frac{1}{2\pi} \sqrt{\frac{\int_{fa}^{fb}(Vobs)^2(f)df}{\int_{fa}^{fb}(Dobs)^2(f)df}} \qquad (4)$$

where $Vobs(f)$ and $Dobs(f)$ are the observed amplitude velocity and displacement spectra corrected for the attenuation effects and related to each other by $Vobs(f) = 2\pi f D_{obs}(f)$.

One of the important parameters of an earthquake source is the stress drop, $\Delta\sigma$, which is defined as the difference of pre-existing tectonic stress and the dynamical frictional stress. For a circular crack of radius r_0, the stress drop $\Delta\sigma$ is given as [32]:

$$\Delta\sigma = 7M_0 / 16 r_0^3 \qquad (5)$$

The other parameter representing the source is its size, which is defined by the radius for circular rupture. The corner frequency f_c of the source spectra is related to the radius r_0 of the equivalent circular crack, which is used to model the earthquake. Such relations have been given by Brune [33-34] as:

$$r_0 = 2.34\beta / 2\pi f_c \qquad (6)$$

where $\rho = 2.8$ g/cm^3 and $\beta = 3.4$ km/s are the mass density and the shear-wave velocity in the vicinity of the earthquake source. We have estimated the seismic moment of the first and second earthquakes as 6.99×10^{25}(dyne-cm) and 4.95×10^{25}(dyne-cm), respectively [35]. The result of f_c, $\Delta\sigma$, r_0 and M_0 are shown in Table (3). Table (4) shows the comparison between results of this study and prior research by Rahimi et al. [36]. They used 110 accelerograms for obtaining source parameters and results have a good adaption.

Table 2. Estimated corner frequency for both events.

Stations	Fc$_1$ (avg)	Fc$_2$ (avg)
Bostan Abad	0.08	0.09
Damirchi	0.09	0.06
Douzal	0.14	0.17
Hoorand	0.15	-
Khajch	0.1	-
Kharvanagh	0.18	0.06
Sofian	0.08	0.09
Tabriz 5	0.1	-
Varzaghan	0.03	0.07
Zanjireh	0.04	-
Khomarloo	0.12	0.15
Mehkin Shahr	0.03	-
Ziveh	0.04	-
Qushchi	0.09	0.12
Lahrood	0.07	0.08
Amand	0.11	0.14
Liqvan	0.09	-
Kaleibar	0.04	0.05
Nir	-	0.07
Tikmedash	-	0.09
Hadi Shahr	0.1	-
Chai Kendy	0.07	-
Seyed Tajedin	0.09	-
Zenoz	-	0.24
Tabriz 6	-	0.15
Avin	-	0.07
Harris	-	0.11
Marand	-	0.15
Nahand	-	0.05

*F_{c1} and F_{c2} are Corner frequencies in the first and second earthquakes, respectively.

Table 3. Estimation of source parameters of the Ahar-Varzeghan earthquakes.

Earthquake	M_w	M_0 (dyne-cm)	r_0 (km)	$\Delta\sigma$ (bar)	f_c (HZ)
First	6.5	6.99×10^{25}	15.83	77.14	0.08
Second	6.4	4.96×10^{25}	11.51	33.06	0.11

Table 4. The important source parameters of earthquakes in the same region by Rahimi et al. [36].

Earthquake	M_0 (dyne-cm)	r_0 (km)	$\Delta\sigma$ (bar)	f_c (HZ)
First	10.9×10^{25}	13.59	86.74	0.13
Second	3.26×10^{25}	8.19	32.02	0.17

According to Tables (3) and (4), as expected radius rupture has inversely proportional to the corner frequency.

4.3. Inversion

Organizing inversion matrix is the first step in the inversion methods. In this article, an inversion scheme is used for obtaining frequency-dependent $Q_\beta(f)$ by using least-squares inversion technique for a nonsingular matrix and singular value decomposition technique for a singular matrix. The advantage of using strong-motion data for the inversion is that it includes valuable high-frequency near-field data suitable for engineering use.

The acceleration spectra of shear waves at a distance R due to an earthquake of seismic moment M_0 can be given as [37-38]:

$$A(f) = C.S(f).D(f) \qquad (7)$$

where C is constant at a particular station for a given earthquake, $S(f)$ represents the source acceleration spectra, and $D(f)$ denotes a frequency-dependent diminution function that modifies the spectral shape and is given as [46]:

$$D(f) = [e^{-\pi f R/Q(f)\beta}/R]P(f, f_m) \qquad (8)$$

In the bracket, the parameter shows the propagation filter and in the preceding equation $P(f, f_m)$ is high-cut filter. In this paper, we have used f_m as 20 Hz. This expression serves as the basis for our inversion. C is constant at a particular station for a given earthquake. For a double-couple seismic source embedded in an elastic medium, considering only S-waves, C is given as:

$$C = M_0 R_{\theta\varphi}.FS.PRTITN/(4\pi\rho\beta^3) \qquad (9)$$

where $R_{\theta\varphi} = 0.55$, is the average shear-wave radiation pattern, $FS = 2$ is the free surface amplification, $PRTITN$ is the reduction factor that accounts for partitioning of energy into two horizontal components and is fixed value 0.707.

In the matrix form, this set of equations can be written as: (subscripts i and j represent the event and the station number, respectively).

This matrix can be represented in the following form:

$$
\begin{vmatrix}
(-\pi\,f1.R11)/\beta & 0 & 0 & . & . & . & . & . & 0 & F(f1, fc1) \\
0 & (-\pi\,f2.R11)/\beta & 0 & . & . & . & . & . & 0 & F(f2, fc1) \\
0 & 0 & (-\pi\,f3.R11)/\beta & . & . & . & . & . & 0 & F(f3, fc1) \\
. & . & . & & & & . & & . & . \\
. & . & . & & & & . & & . & . \\
0 & 0 & 0 & . & . & . & . & . & (-\pi\,fn.R11)/\beta & F(fn, fc1) \\
(-\pi\,f1.R12)/\beta & 0 & 0 & . & . & . & . & . & 0 & F(f1, fc1) \\
0 & (-\pi\,f2.R12)/\beta & 0 & . & . & . & . & . & 0 & F(f2, fc1) \\
0 & 0 & (-\pi\,f3.R12)/\beta & . & . & . & . & . & 0 & F(f3, fc1) \\
. & . & . & & & & . & & . & . \\
0 & 0 & 0 & . & . & . & . & . & (-\pi\,fn.R12)/\beta & F(fn, fc1) \\
& & & & & & . & & & . \\
& & & & for\ \ mth\ \ earthquake & & . & & & . \\
(-\pi\,f1.Rm1)/\beta & 0 & 0 & . & . & . & . & . & 0 & F(f1, fcm) \\
0 & (-\pi\,f2.Rm1)/\beta & 0 & . & . & . & . & . & 0 & F(f2, fcm) \\
0 & 0 & (-\pi\,f3.Rm1)/\beta & . & . & . & . & . & 0 & F(f3, fcm) \\
. & . & . & & & & . & & . & . \\
. & . & . & & & & . & & . & . \\
0 & 0 & 0 & . & . & . & . & . & (-\pi\,fn.Rm1)/\beta & F(fn, fcm) \\
(-\pi\,f1.Rm2)/\beta & 0 & 0 & . & . & . & . & . & 0 & F(f1, fcm) \\
0 & (-\pi\,f2.Rm2)/\beta & 0 & . & . & . & . & . & 0 & F(f2, fcm) \\
0 & 0 & (-\pi\,f3.Rm2)/\beta & . & . & . & . & . & 0 & F(f3, fcm) \\
. & . & . & . & . & . & . & . & . & . \\
. & . & . & . & . & . & . & . & . & . \\
0 & 0 & 0 & . & . & . & . & . & (-\pi\,fn.Rm2)/\beta & F(fn, fcm)
\end{vmatrix}
\begin{vmatrix}
1/Q\beta(f1) \\
1/Q\beta(f2) \\
1/Q\beta(f3) \\
. \\
. \\
. \\
. \\
. \\
. \\
. \\
. \\
. \\
. \\
. \\
. \\
. \\
. \\
. \\
. \\
. \\
. \\
1/Q\beta(fn) \\
\Delta fc
\end{vmatrix}
=
\begin{vmatrix}
D11(f1) \\
D11(f2) \\
D11(f3) \\
. \\
. \\
D11(fn) \\
D12(f1) \\
D12(f2) \\
D12(f3) \\
. \\
D12(fn) \\
. \\
. \\
Dm1(f1) \\
Dm1(f2) \\
Dm1(f3) \\
. \\
. \\
Dm1(fn) \\
Dm2(f1) \\
Dm2(f2) \\
Dm2(f3) \\
. \\
. \\
Dm2(fn)
\end{vmatrix}
$$

$$GM = d \tag{10}$$

Model parameters are contained in the model matrix M, and the spectral component is in the data matrix d. Inversion of the G matrix using the Newton method gives the model matrix M as:

$$M^{est} = (GTG)^{-1} G^T d \tag{11}$$

The corner frequency is treated as the input parameter in the inversion algorithm to maintain the linearity in Equation (9). Different solutions were obtained for different possibilities of f_c. The final solution is obtained corresponding to minimum RMSE. In the present inversion scheme, several possibilities of corner frequencies are checked by iteratively changing the corner frequency f_c in an increment of Δf. The small increment Δf considered in the present work is 0.2 Hz. The inversion resulting in Equation (11) is prone to problems if GTG is even close to singular, and in such a case, singular value decomposition is used to solve Equation (11) (Press et al. [47]).

Matrix (M^{est}) illustrate $1/Q_0$ for every frequency, in this study used frequency band between 1 to 20 HZ, 0.2 steps so we have 96 frequencies with 96 values of Q for each station. After that estimate total Q factor for every station that available in Table (5); therefore, inversion function should be repeated 40 times until calculate all of stations' Q-values. In the next stage, by having 40 $Q_\beta(f)$ it is necessary to estimate a comprehensive value for all areas. In order to achieve this goal, all of the stations in some selected frequencies in Table (6) should be plotted with their standard deviation to show errors in frequencies.

5. Results and Discussion

For the 2012 Ahar-Varzeghan earthquakes, Yaghmaei-Sabegh [39] studied the strong-motion records. Zafarani et al. [18] employed stochastic simulation of strong-motion records and generalized inversion of S-wave amplitude spectra for deriving the site response and S-wave attenuation from the 2012 Ahar-Varzeghan doublet earthquakes. They found the optimum average stress parameter associated with the first and second earthquakes as 100 and 130 bars, frequency-dependent S-wave quality factor, $Q_s = 99f^{0.77}$, similarity in the shape of site response spectra using both the H/V and generalized inversion method.

Table 5. Q_β (f) for all stations of the two events.

Stations	$Q_\beta(f)$ (First Event)	$Q_\beta(f)$ (Second Event)
Bostan Abad	$Q_\beta(f) = 103f^{0.73}$	$Q_\beta(f) = 97f^{0.82}$
Damirchi	$Q_\beta(f) = 75f^{0.91}$	$Q_\beta(f) = 81f^{0.85}$
Douzal	$Q_\beta(f) = 77f^{0.93}$	$Q_\beta(f) = 85f^{0.92}$
Hoorand	$Q_\beta(f) = 74f^{0.86}$	-
Khajch	$Q_\beta(f) = 68f^{0.81}$	-
Kharvanagh	$Q_\beta(f) = 72f^{0.78}$	$Q_\beta(f) = 73f^{0.69}$
Sofian	$Q_\beta(f) = 107f^{0.76}$	$Q_\beta(f) = 104f^{0.79}$
Tabriz 5	$Q_\beta(f) = 96f^{0.77}$	-
Varzaghan	$Q_\beta(f) = 40f^{0.78}$	$Q_\beta(f) = 46f^{0.73}$
Zanjireh	$Q_\beta(f) = 143f^{0.79}$	-
Khomarloo	$Q_\beta(f) = 103f^{0.79}$	$Q_\beta(f) = 108f^{0.80}$
Mehkin Shahr	$Q_\beta(f) = 106f^{0.80}$	-
Ziveh	$Q_\beta(f) = 119f^{0.78}$	-
Qushchi	$Q_\beta(f) = 152f^{0.86}$	$Q_\beta(f) = 162f^{0.83}$
Lahrood	$Q_\beta(f) = 98f^{0.83}$	$Q_\beta(f) = 95f^{0.85}$
Amand	$Q_\beta(f) = 90f^{0.84}$	$Q_\beta(f) = 112f^{0.78}$
Liqvan	$Q_\beta(f) = 126f^{0.74}$	-
Kaleibar	$Q_\beta(f) = 58f^{0.93}$	$Q_\beta(f) = 63f^{0.89}$
Harris	-	$Q_\beta(f) = 56f^{0.78}$
Marand	-	$Q_\beta(f) = 110f^{0.93}$
Nahand	-	$Q_\beta(f) = 63f^{0.73}$
Nir	-	$Q_\beta(f) = 124f^{0.81}$
Tikmedash	-	$Q_\beta(f) = 108f^{0.79}$
Hadi Shahr	$Q_\beta(f) = 74f^{0.84}$	-
Chai Kendy	$Q_\beta(f) = 53f^{0.85}$	-
Seyed Tajedin	$Q_\beta(f) = 149f^{0.80}$	-
Zenoz	-	$Q_\beta(f) = 107f^{0.86}$
Tabriz 6	-	$Q_\beta(f) = 71f^{0.87}$
Avin	-	$Q_\beta(f) = 127f^{0.88}$

Table 6. Average of Q_β (f) and standard deviation in mentioned frequencies for both earthquakes.

Frequency	Q-avg Total	STDV Total	Q Event1	STDV Event1	Q Event2	STDV Event2
1	96	29	95	31	94	28
3	232	73	231	73	233	75
7	468	171	464	144	470	163
10	629	205	621	193	632	227
13	782	259	771	240	786	289
16	929	311	915	286	934	350
20	1118	380	1100	346	1125	431

By implementing inversion on records, the average $Q(f)$ relationship is obtained by using the average of Q_β values. The average values of $Q_\beta(f)$ for region stations are given in Table (5). The iterative inversion was performed at each station independently.

Figure (5) shows an example of a selected portions of the shear wave (4 s) and the source spectra of the first Ahar-Varzeghan earthquake ($Mw = 6.4$), as used for the inversion, and comparisons of the source spectra from the corrected records and those from the Brune's model in three different stations of Sofian, Tabriz and Harris, respectively.

Figures (6) and (7) show the average plot of Q at different frequencies (1-20 HZ) with the regression lines from the least-squares estimation with respect to the first and second events. Lower Q_β values can be observed for near main shock epicenter stations (i.e. Varzeghan, $Q_0=40$) and higher Q_β values for distant stations (i.e. Qushchi, $Q_0=162$) (Table 7). The experimental results show that the quality factor Q is affected significantly by the presence of cracks, and therefore, it is extremely cracking sensitive. The environment of the epicenter is more affected by the released energy and seismic waves recorded in the near-field are propagated in the filled crack area. To better understand this section, Figure (8) that
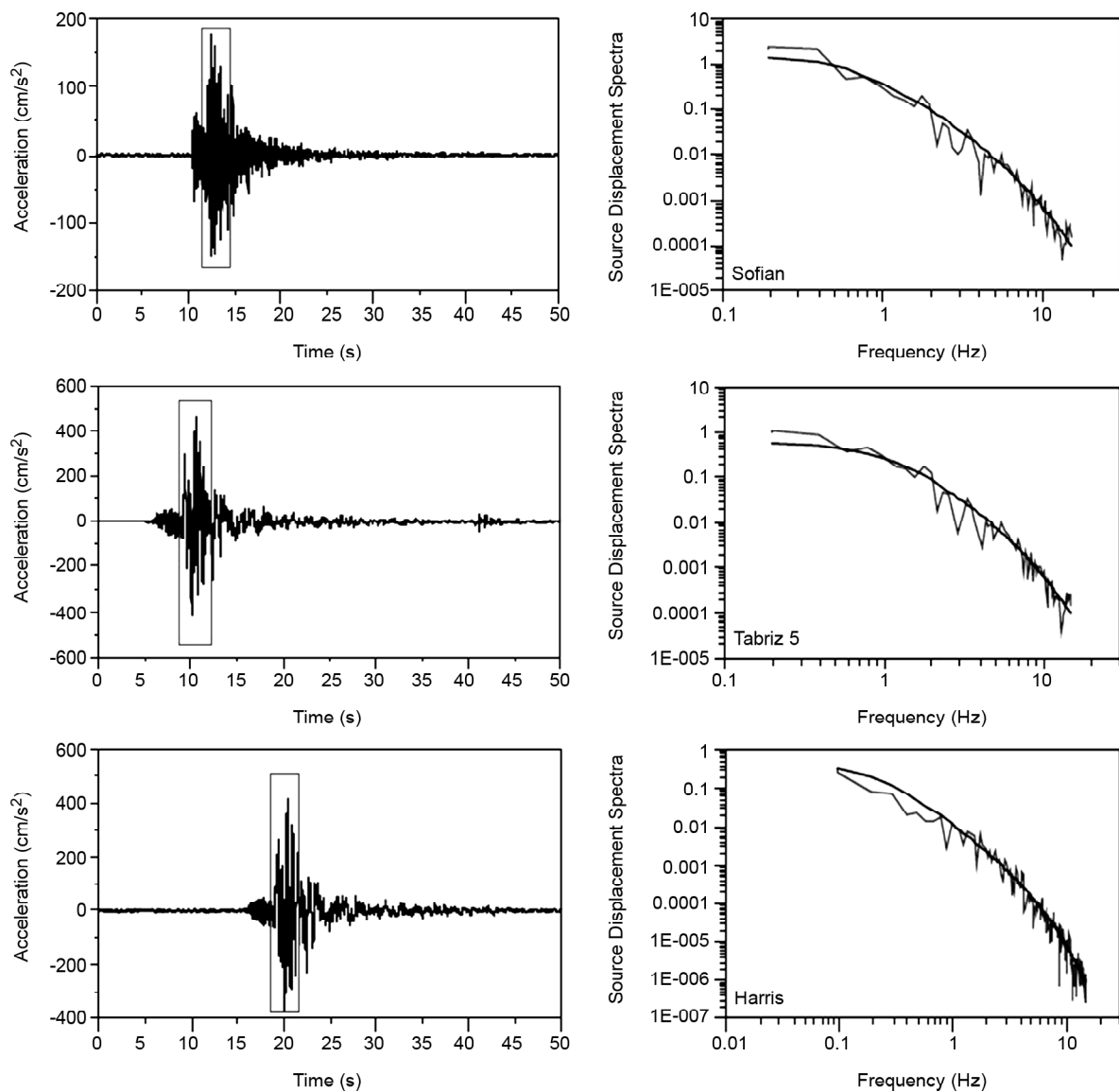

Figure 5. Selected portions of the vertical component of the accelerograms of the Ahar-Varzeghan earthquake, as used for the inversion, and comparisons of the source spectra from the corrected records and those from the Brune model (see the acceleration records at left hand in the Sofian, Tabriz 5 and Harris stations, and the source spectra at the right hand); the thick solid line shows the theoretical Brune's spectrum, and the spectrum from the observed record is shown by the thin dark line.
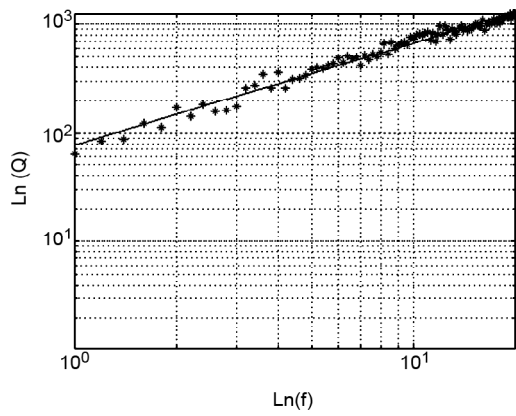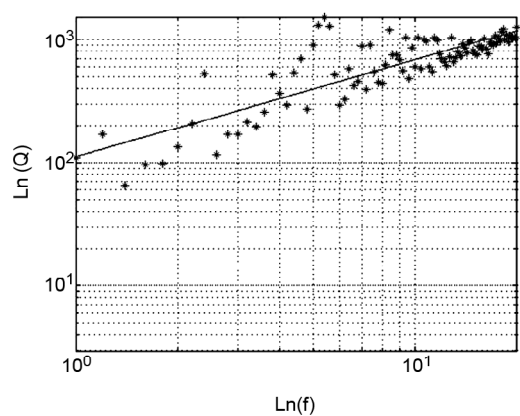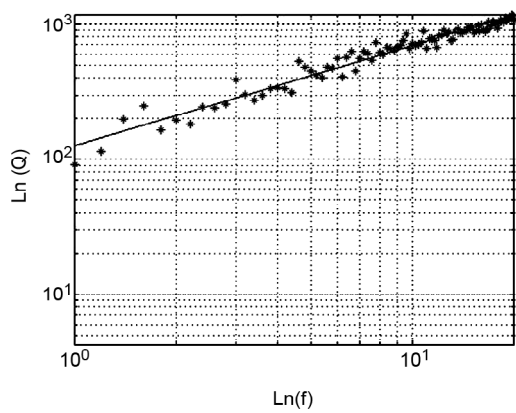
(a) Douzal Station; $Q_\beta(f) = 77f^{0.93}$
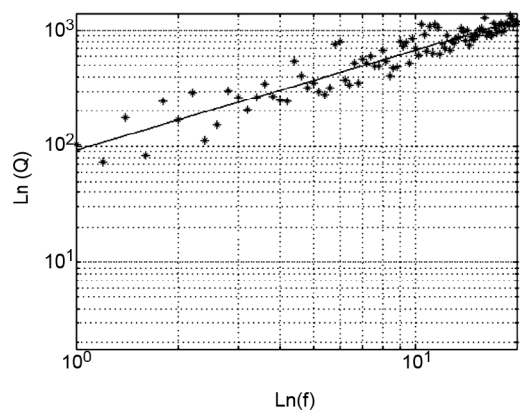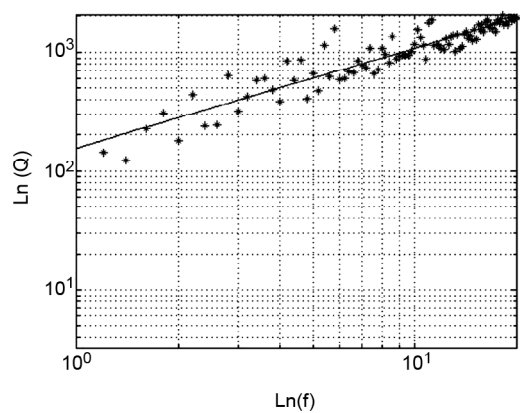

(a) Bostan Abad Station; $Q_\beta(f) = 97f^{0.82}$
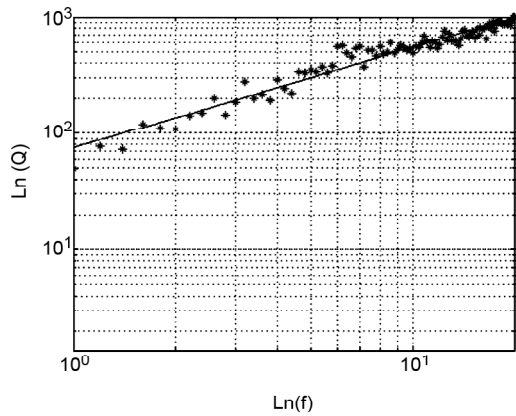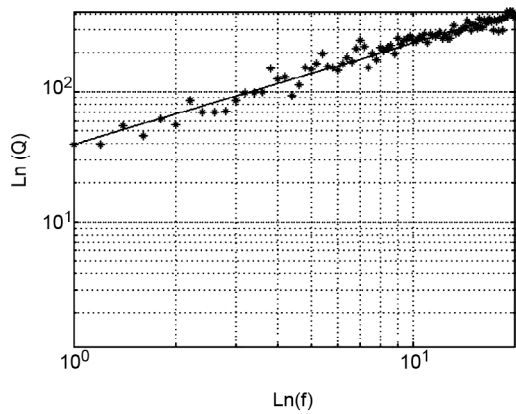

(b) Hoorand Station; $Q_\beta(f) = 74f^{0.86}$

(b) Khomarloo Station; $Q_\beta(f) = 108f^{0.8}$
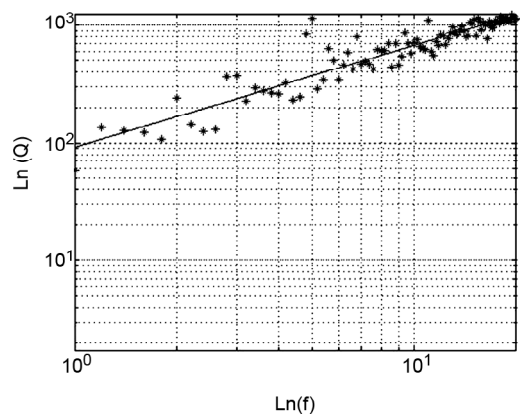

(c) Liqvan Station; $Q_\beta(f) = 126f^{0.74}$

(c) Qushchi Station; $Q_\beta(f) = 162f^{0.83}$

(d) Varzaghan Station; $Q_\beta(f) = 40f^{0.78}$

(d) Lahrood Station; $Q_\beta(f) = 95f^{0.85}$

Figure 6. The rate of change of Q_β versus Frequency in four stations of Ahar earthquake and their equations.

Figure 7. The rate of change of Q_β versus frequency in four stations of Varzeghan earthquake and their equations.
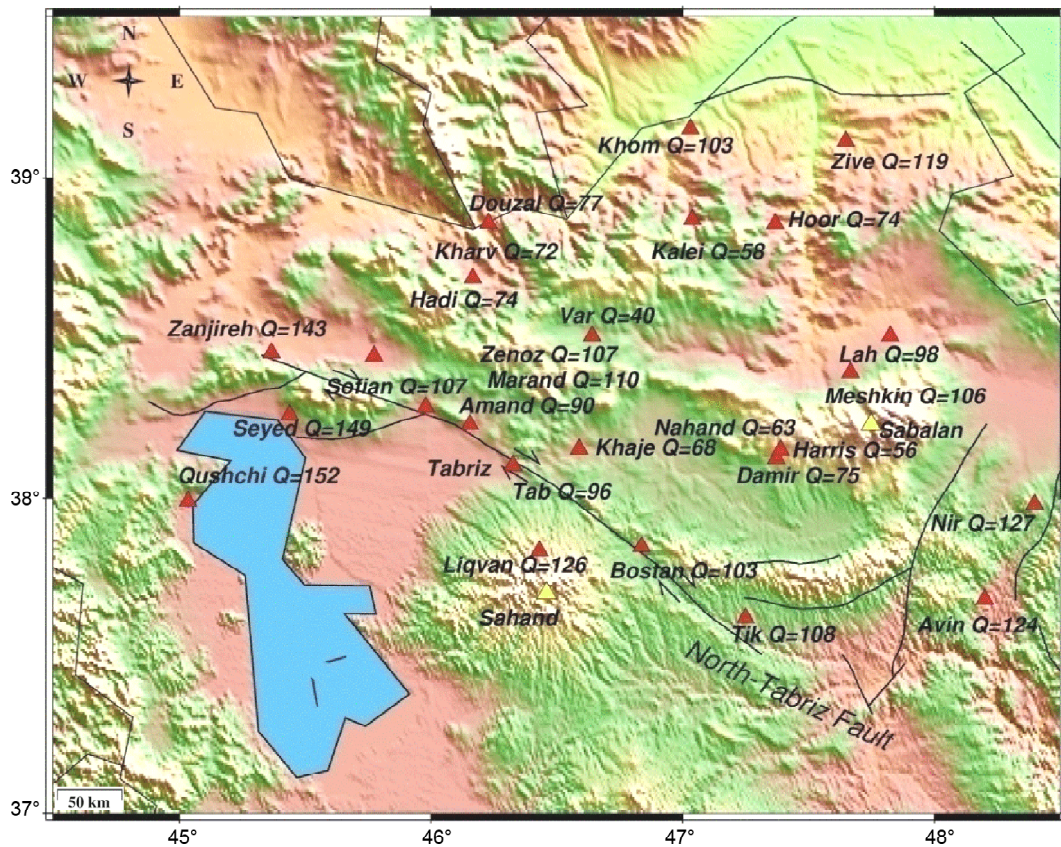
Figure 8. Distribution of Q values in all stations.

Table 7. Examples of some stations to illustrate a direct relation-ship between the station-epicenter distance (R) and Q parameter.

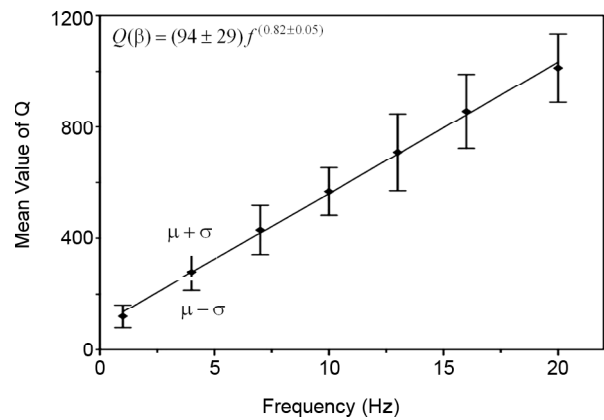| Station	R(KM)	Q_0
Qushchi	169.85	152
Seyed Tajedin	159.57	149
Avin	121.64	127
Liqvan	85.05	126
Tabriz 5	65.74	96
Hoorand	58	74
Nahand	45.5	63
Kaleibar	41.09	58
Harris	39.03	56
Varzeghan	19.19	40

Figure 9. Regional $Q_\beta(f)$ relationship for NW-Iran based on the obtained value of shear wave attenuation at different stations at different frequencies.

illustrates distribution of Q value in this region will be helpful.

The plot of average $Q(f)$ values versus frequency is shown in Figure (9). In order to calculate regional $Q(f)$ relation, the mean values of Q_β at each frequency and different stations (Tables 5 and 6), obtained from inversion is plotted in Figure (9). The best fit line gives $Q(f) = (94 \pm 29)\, f^{(0.82 \pm 0.05)}$ that represents regional attenuation characteristics of

NW-Iran.

It would be more appropriated to compare it with other regions in order to observe whether characteristics are present in the study area. As a result of tectonic differences in active regions, such linear relations have a different slope relative to the relation applied in the other regions and consequently each region needs a specific relation. Figure (10) shows the comparison of this study with the other
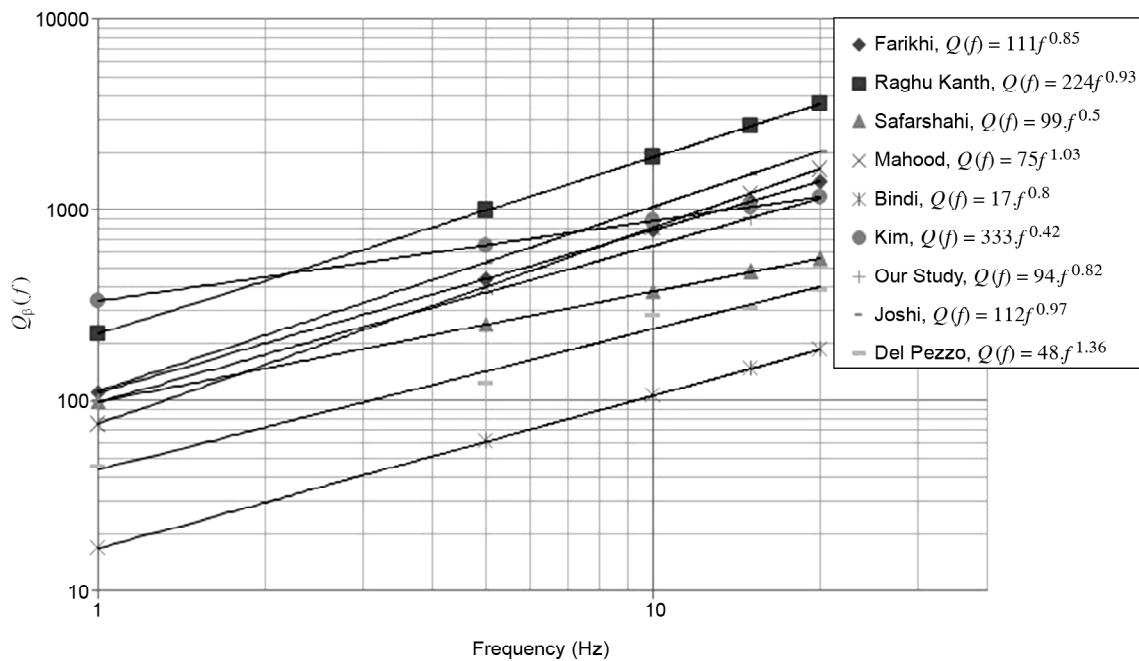
Figure 10. Comparison of obtained $Q_\beta(f)$ with other relations from seismically active regions.

regions. The obtained relation is similar to the relation developed for seismically active regions.

6. Conclusion

The strong-motion data of the two earthquakes of Ahar-Varzeghan have been used in inversion to estimate the frequency-dependent attenuation relation $Q_\beta(f)$. In this study, the minimum error is obtained in the inversion scheme for a relation that gives $Q_\beta = (94 \pm 29) f^{(0.82 \pm 0.05)}$. Furthermore, by comparing with other studies such as Alborz, Eastern Iran and Himalaya regions, NW-Iran introduced as an active area with low Q-value amongst other zones. This result can be arisen from the existence of the two volcanoes in this zone that provide effective hydrothermal currents in sub surfaces. Seismic attenuation has been studied on numerous volcanoes. For example, Del Pezzo et al. [20] measured the attenuation in Etna and Andalucia volcanoes (south of Spain) $Q(f) = 48f1.36$. The results show that Q, the absolute characteristic values of volcanoes are slightly smaller than those measured in non-volcanic zones, and sometimes their frequency dependency is different.

Moreover, it is interesting to note that our results have great coincidence with Zafarani et al. [18] outcomes that was equaled with $Q_\beta = (99 \pm 1) f^{(0.77 \pm 0.01)}$ in terms of quality factor value.

The inversion scheme also gives the estimate of the corner frequencies for the earthquakes, which gives stress-drop values for these earthquakes at 77.14 and 33.06 bars, respectively, which very well matches with other observations.

References

1. Mahood, M. (2014) Attenuation of high-frequency seismic waves in Eastern Iran. *Pure Appl. Geophysics*, **171**, 2225-2240.

2. Sato, H., Fehler, M.C., and Maeda, T. (2012). 'Tectonic seismology'. In: *Seismic wave propagation and scattering in the heterogeneous earth*, **496**, Springer, Berlin, Page 494.

3. Joshi, A. (2006) Use of acceleration spectra for determining the frequency-dependent attenuation coefficient and source parameters. *Bulletin of the Seismological Society of America*, **96**(6), 2165-2180.

4. Joshi, A., Kumar, C., Lomnitz, H., Castanos, and

Akhtar, S. (2012) Applicability of attenuation relations for regional studies. *Geofisical Internacional*, **51**, 349-363.

5. Kumar, A. and Mittal, H. (2015) Earthquake source parameters review in Indian context. *Int. J. Civil Struct. Environ,* **3**(1), 41-52.

6. Aki, K. (1980) Attenuation of shear-waves in the lithosphere for frequencies from 0.05 to 25 Hz. *Phys. Earth Planet. Inter.*, **21**, 50-60.

7. Kumar, N., Parvez, I.A., and Virk, H.S. (2005) Estimation of coda wave attenuation for NW Himalayan region using local earthquakes. *Phys. Earth Planet. Inter.*, **151**, 243-258.

8. Mahood, M. and Hamzehloo, H. (2009) Estimation of coda wave attenuation in East Central Iran. *J. Seismol.*, **13**, 129-139.

9. Erickson, D., McNamara, D.E., and Benz, H.M. (2004) Frequency dependent LgQ within the continental United States. *Bull. Seismol. Soc. Am.*, **94**(5), 1630-1643.

10. Benz, H., Frankel, A., and Boore, D. (1997) Regional Lg attenuation for the continental United States. *Bull. Seismol. Soc. Am.*, **87**, 606-619.

11. Farrokhi, M., Hamzehloo, H., Rahimi, H., and Allameh Zadeh, M. (2016) Estimation of coda wave attenuation in the central and eastern Alborz, Iran. *Bull. Seis. Soc. Am.*, **106**, 1482-1498.

12. Mahood, M. and Hamzehloo, H. (2011) Variation of intrinsic andscattering attenuation of seismic waves with depth in the Bamregion, East-Central Iran. *Soil Dynamics and Earthquake Engineering*, **31**, 1338-1346.

13. Zafarani, H., Hassani, B., and Ansari, A. (2012) Estimation of earthquake parameters in the Alborz seismic zone, Iran using generalized inversion method. *Soil Dynam. Earthq. Eng.*, **42**, 197-218.

14. Hassani, B., Zafarani, H., Farjoodi, J., and Ansari, A. (2011) Estimation of site amplification, attenuation and source spectra of S-waves in the East-Central Iran. *Soil Dynamics and Earthquake Engineering*, **31**, 1397-1413.

15. Motaghi, K. and Ghods, A. (2012) Attenuation of ground-motion spectral amplitudes and its variations across the central Alborz mountains. *Bull. Seism. Soc. Am.*, **102**, 1417-1428.

16. Rahimi, H., Motaghi, K., Mukhopadhyay, S., and Hamzehloo, H. (2010) Variation of coda wave attenuation in the Alborz region and central Iran. *Geophys. J. Int.*, **181**, 1643-1654.

17. Farrokhi, M. and Hamzehloo, H. (2015) Attenuation of high frequency P and S waves in the crust of Alborz region, Iran. *Geophys. J. Int.*, **188**, 645-679.

18. Zafarani, H., Rahimi, M., Noorzad, A., Hassani, B., and Khazaei, B. (2015) Stochastic simulation of strong-motion records from the 2012 Ahar-Varzeghan dual earthquakes, Northwest of Iran. *Bull. Seism. Soc. Am.*, **153**, 489-502.

Andrews, D.J. (1986) Objective determination of source parameters and similarity of earthquakes of different size, Earthq. *Source Mech. American Geophysical Union*, **37**, 259-267.

19. Del Pezzo, E., Bianco, F., and Zaccarelli, L. (2006) Separation of Qi and Qs from passive data at Mt. Vesuvius: a reappraisal of the seismic attenuation estimates. *Phys. Earth Planet. Int.*, **159**, 202-212.

20. Vernant, Ph., Nilforoushan, F., Hatzfeld, D., Abbassi, M.R., Vigny, C., Masson, F., Nankali, H., Martinod, J., Ashtiani, A., Bayer, R., Tavakoli, F., and Chéry, J. (2004) Present-day crustal deformation and plate kinematics in the middle east constrained by GPS measurements in Iran and northern Oman. *Geophys. J. Int.*, **157**, 381-398.

21. Jackson, J. (1992) Partitioning of strike-slip and convergent motion between Eurasia and Arabia in eastern Turkey and the Caucasus. *J. Geophys. Res.*, **97**, 12471-12479.

22. McClusky, S., Balassanian, S., Barka, A., Demir, C., Ergintav, S., Georgiev, I., Gurkan, O., Hamburger, M., Hurst, K., Kahle, H., Kastens, K., Kekelidze, G., King, R., Kotzev, V., Lenk, O., Mahmoud, S., Mishin, A., Nadariya, M., Ouzounis, A., Paradissis, D., Peter, Y., Prilepin, M., Reilinger,

R., Sanli, I., Seeger, H., Tealeb, A., Toksoz, M.N., and Veis, G. (2000) Global positioning system constraints on plate kinematics and dynamics in the eastern Mediterranean and Caucasus. *J. Geophys. Res.,* **105**, 5695-5719.

24. Copley, A. and Jackson, J. (2006) Active tectonics of the Turkish-Iranian plateau. *Tectonics*, **25**, 165-166.

25. Masson, F., Djamour, Y., Van Gorp, S., Chery, J., Tatar, M., Tavakoli, F., Nankali, H., and Vernant, P. (2006) Extension in NW Iran driven by the motion of the South Caspian Basin. *Earth planet. Sci. Lett.*, **252**, 180-188.

26. Reilinger, R., McClusky, S., Vernant, Ph., Lawrence, Sh., Ergintav, S., Cakmak, R., Ozener, H., Kadirov, F., Guliev, I., Stepanyan, R., Nadariya, M., Hahubia, G., Mahmoud, S., Sakr, K., ArRajehi, A., Paradissis, D., Al-Aydrus, A., Prilepin, M., Guseva, T., Evren, E., Dmitrotsa, A., Filikov, S.V., Gomez, F., Al-Ghazzi, R., and Karam, G. (2006) GPS constraints on continental deformation in the Africa-Arabia-Eurasia continental collision zone and implications for the dynamics of plate interactions. *J. Geophys. Res.*, **111**, 5411.

27. Djamour, Y., Vernant, P., Nankali, H.R., and Tavakoli, F. (2011) NW Iran eastern Turkey present-data kinematics: results from the Iranian permanent GPS network. Earth Planet. *Sci. Lett.*, **307**, 27-34.

28. Razzaghi, M.S. and Ghafory-Ashtiany, M. (2012) A preliminary reconnaissance report on August 11th 2012, Varzeghan-Ahar twin earthquakes. *Report of International Association of Seismology and Physics of the Earth's Interior*, **9**, 78-89.

29. Xu, Z. and Schwartz, S.Y. (1993) Large earthquake doublets and fault plane heterogeneity in the northern Solomon Islands subduction zone. *Pure Appl. Geophys.*, **140**, 365-390.

30. Yoshimoto, K., Sato, H., and Ohtake, M. (1993) Frequency-dependent attenuation of P and S waves in the Kanto area, Japan, based on the coda normalization method, *Geophys. J. Int.*, **114**, 165-174.

31. Kinoshita, S. (1994) Frequency-dependent attenu

ation of shear waves in the crust of the southern Kanto area, Japan. *Bull. Seism. Soc. Am.*, **84**, 1387-1396.

32. Papageorgiou, A.S. and Aki, K. (1983) A specific barrier model for the quantitative description of inhomogeneous faulting and the prediction of strong ground motion, Part I: Description of the model. *Bull. Seismol. Soc. Am.*, **73**, 693-722.

33. Brune, J.N. (1970) Tectonic stress and the spectra of seismic shear waves from earthquakes. *J. Geophys. Res.*, **75**, 4997-5009.

34. Brune, J.N. (1971) Correction. *J. Geophys. Res.*, **76**, 5002.

35. Hanks, T.C. and Kanamori, H. (1979) A moment magnitude scale. *J. Geophys. Res.*, **84**, 2348-2350.

36. Rahimi, H., Masominia, N., and Rezapour, M. (2013) Estimation of the kinematic source parameters and frequency independent shear wave Quality factor from acceleration records of the Ahar-Varzeghan earthquake 2012. *Journal of Physics of the Earth and Space*, **26**, 483-502.

37. Boore, D.M. (1983) Stochastic simulation of high-frequency ground motions based on seismological models of the radiated spectra. *Bull. Seismol. Soc. Am.*, **73**, 1865-1894.

38. Atkinson, G. and Boore, D.M. (1998) Evaluation of models for earthquake source spectra in eastern North America. *Bull. Seismol. Soc. Am.*, **88**, 917-934.

39. Yaghmaei-Sabegh, S. (2014) Time-frequency analysis of the 2012 double earthquakes records in north-west of Iran. *Bull. Earthq. Eng.*, **12**, 585-606.

40. Kim, K.D., Chung, T.W., and Kyung, J.B. (2004) Attenuation of high-frequency P and S waves in the crust of Choong Chung Islands, central South Korea. *Bull. Seis. Soc. Am.*, **94**, 1070-1078.

41. Safarshahi, M., Rezapour, M., and Hamzehloo, H. (2013) Stochastic finite-fault modeling of ground motion for the 2010 Rigan Earthquake,

Southeastern Iran. *Bull. Seism. Soc. Am.*, **103**, 223-235.

42. Joshi, A. (2007) Inversion of seismic intensity data for the determination of three-dimensional attenuation structures in the central gap region of Himalayas. *Nat. Hazards*, **43**, 129-146.

43. Bindi, D., Parolai, H., Grosser, C., and Karakisa, S. (2006) Crustal attenuation characteristics in northwestern Turkey in the range from 1 to 10 Hz. *Bull. Seism. Soc. Am.*, 96, 200-214.

44. Elliott, J.R. Copley, A.C., Holley, R., Scharer, K., and Parsons, B. (2013) The 2011 Mw 7.1 Van (Eastern-Turkey) earthquake. *J. Geophys. Res. Solid Earth*, **118**, 1619-1637.

45. Jackson, I., Fitz Gerald, J.D., Faul, H., and Tan, B.H. (2002) Grain-size sensitive seismic wave attenuation in polycrystalline olivine. *J. Geophys. Res.*, **107**(B12), 2360.

46. Boore, D. and Atkinson, G. (1987) Stochastic prediction of ground motion and spectral response parameters at hard-rock sites in eastern North America. *Bull. Seism. Soc. Am.*, **77**, 440-467.

47. Press, W.H., Teukolsky, S.A., Vetterling, W.T., and Flannery, B.P. (1992) 'Numerical Recipes in Fortran.' In: *The Art of Scientific Computing*. 2nd ed. Cambridge University Press, Cambridge, UK, 340-359.